International Journal of Science and Engineering Applications
Volume 7–Issue 02, 01-07, 2018, ISSN:-2319–7560

Seismic Vulnerability Assessment of Coupled Wall RC Structures

Ramin Taghinezhad
Research Assistant
Department of Civil and Environmental Engineering
Florida International University
USA

Arash Taghinezhad
Graduate Research Assistant
Department of Construction Management
Louisiana State University
USA

Vahid Mahdavifar (PI)
Post-doctoral Research Associate
Department of Environmental Conservation
University of Massachusetts
Amherst, USA

Vafa Soltangharaei
Graduate Research Assistant
Department of Civil and Environmental Engineering
University of South Carolina
USA

Abstract: Swiss Federal Institute of Technology developed a simple method to evaluate seismic vulnerability of reinforced concrete buildings with structural walls using an engineering approach. The objective of this research was the evaluation of the developed method through the capacity curve with a focus on the buildings with frame action due to the coupling of the walls by piers and spandrels. For this purpose, a numerical model of a six-story reinforced concrete structure with sixteen structural walls was created in two directions and nonlinear static analysis was performed to obtain the capacity curve under different lateral load patterns. It was found that there is an appropriate overlap between the numerical model and developed method in terms of capacity curve and vulnerability.

Keywords: concrete, nonlinear static analysis, reinforced concrete buildings, seismic vulnerability, structural shear wall,

1. INTRODUCTION

Reinforced concrete structures with the structural walls are often classified into three types: structural wall systems with negligible frame action, Structural wall systems with separate frame action, and structural wall systems with frame action due to the coupling of the walls [1]. The first type includes slender reinforced concrete walls, which carry lateral loads and columns carry gravity loads without frame-wall interaction. In the second type, a moment resisting frame is created in the structure by rigid connections between beams and columns, and the structural walls carry lateral loads. The third type consists of structural walls that carry both gravity and lateral forces. There are no gravity columns in this system. In fact, the

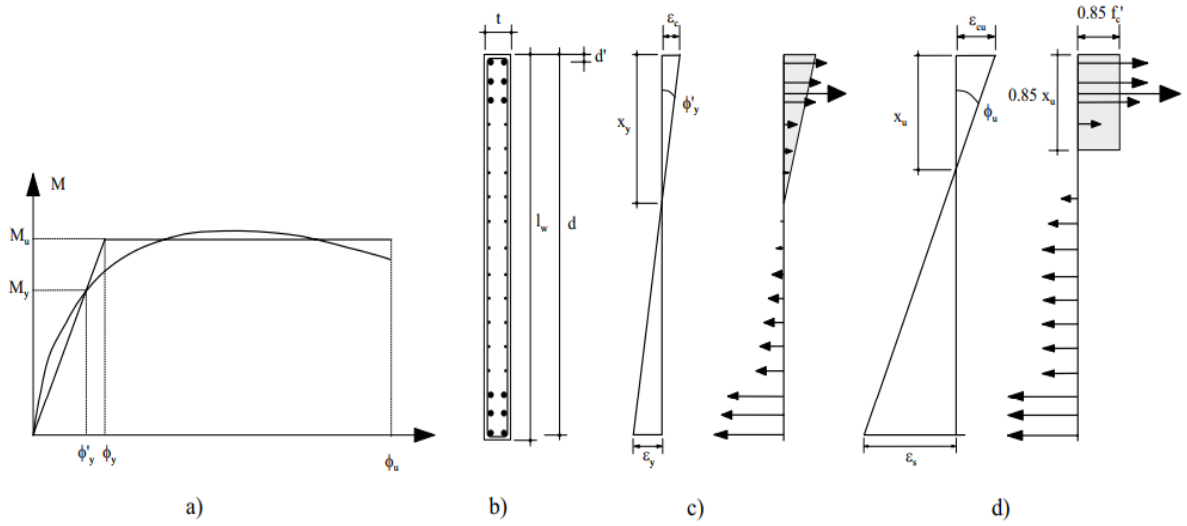

Figure 1: (a) Bilinear moment-curvature diagram, (b) wall section, (c) strain and force diagram on initial yielding, and (d) strain and force diagram in the ultimate level [1].

coupling between pier and spandrel carries lateral forces. Structural walls are also would potentially be arranged in a network of walls interconnected with each other to make a rigid box which is called shear core wall. The core is used to provide lateral stiffness required for the buildings in concrete frame structures [2] or non-concrete structures such as mass timber buildings [3, 4].

In this paper, in addition to outlining the vulnerability assessment of the third type of structural wall systems, presented by Swiss Federal Institute of Technology [1], an example of this type of structures was given and evaluated using nonlinear static analysis. To this end, structure capacity curves were derived using the analytical method. Generally, two methodologies can be utilized for deriving capacity curves: experimental and analytical. Two analytical methods of incremental nonlinear time history and nonlinear static (pushover) analysis are recommended for this purpose. Some researchers extracted the capacity curves of multi-story structures using incremental time history analyses [5-10] Several time history analyses were conducted by applying different earthquake acceleration records and with different intensity scales. Although this method presents more realistic behavior of structures, it is very time consuming and more sensitive to the modeling and analytical parameters. Therefore, review of the literature reveals that nonlinear static analyses have gained more practical application instead of the nonlinear time history analysis [11-19]. To derive capacity curve in experimental tests, the loading increase step by step at the location of force until the final collapse of the structure or major drop in strength [20-21]. In this study, the nonlinear static analysis was employed to derive the capacity curves of a reinforced concrete structure. Finally, a comparison between results from nonlinear static analysis and developed method by Swiss Federal Institute of Technology was made.

2. METHODOLOGY

2.1 Moment-Curvature Equation in the Reinforced Concrete Wall Section

In concrete wall sections, with the distribution of the reinforcement throughout the cross-section, moment-curvature equations can be roughly drawn as bilinear curves as described in Fig. 1. This curve is characterized by two points: (φ'_y, M_y) which indicates the first yield of tensile reinforcement, and (φ_u, M_u) indicates the ultimate compressive flexural strength of concrete. The curvature of the first yield can be determined from the following equation according to (Fig.1 (c)):

$$\varphi'_y = \frac{\varepsilon_y}{d - X_y} \qquad (1)$$

$\varepsilon_y = f_y / E_S$: Yield Strain of the reinforcement

f_y : Yield strength of the reinforcement

E_s : Elastic modulus of elasticity in the reinforcement

d : Distance from compression face to tension reinforcement,

X_y : Neutral axial depth

The final curvature φ_u is also determined from the following equation (Fig. 1 (d)):

$$\varphi_u = \frac{\varepsilon_{cu}}{X_u} \qquad (2)$$

ε_{cu} : The final compression strain in the concrete

X_u : Neutral axial depth.

According to Fig. 1, the nominal yield curvature and ductility of the wall section are also defined as follows:

$$\varphi_y = \varphi'_y \frac{M_u}{M_y}, \quad \mu_\varphi = \frac{\varphi_u}{\varphi_y} \qquad (3)$$

According to Fig. 1 and curvature in a structural wall ($\varphi = M / EI$), the yielding displacement at the top of the wall for different force distributions is obtained from:

$$\Delta_y = \chi \varphi_y H_{tot}^2 \qquad (4)$$

In the force distribution which is close to the first mode, the coefficient χ is varied from 0.17 for the single force at top and 0.276 for the triangular force distribution, once $\chi = 0.2$ was suggested [1]. The final displacement at the top of the wall is also obtained from the following equation:

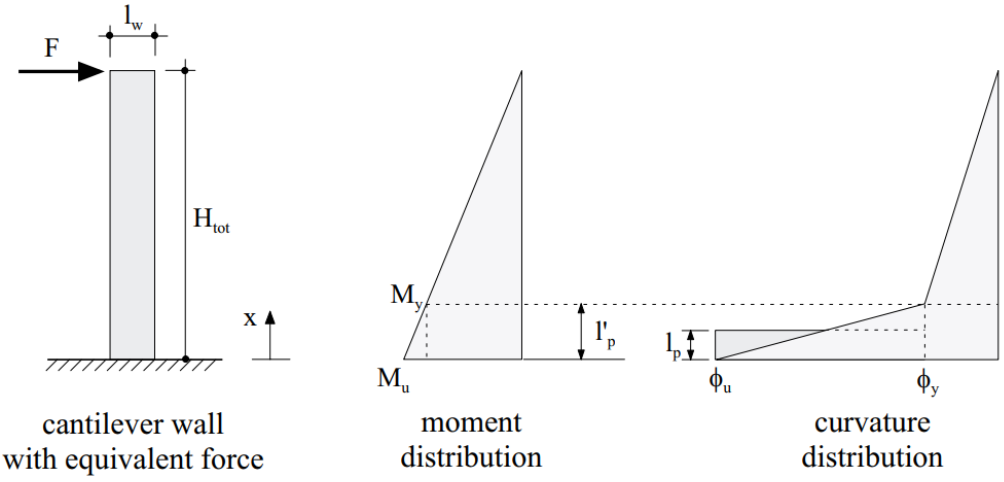

Figure 2: Cantilever wall under single horizontal force and distribution of moment and curvature [1].

$$\Delta_u = \mu_w \Delta_y \quad (5)$$

μ_w is the ductility of a wall and it is expressed as follows in terms of μ_φ :

$$\mu_w = 1 + \frac{1}{\chi H_{tot}^{\ 2}}(\mu_\varphi - 1) l_p (H_{tot} - \frac{l_p}{2}) \quad (6)$$

According to Fig. 2, which shows a moment-curvature curve for a wall with a single horizontal force, $l_p^{'}$ is the height of the wall that the reinforcement starts to yield, in another word, it is the height with the yielding moment ($M(x) = M_y$). Therefore, in the length of the wall where nonlinearity starts to develop. This length is called l_p or the length of the plastic hinge.

$$M(x = l_p) = M_Y = M_u (1 - \frac{l_p}{H_{tot}}) \quad (7)$$

Assuming linear expansion of curvature from φ_y to φ_u :

$$l_p = \frac{H_{tot}}{2}(1 - \frac{M_y}{M_u}) \quad (8)$$

In the triangular distribution of lateral force, Eq. (9) is expressed as follows [1]:

$$M(x = l_p) = M_y = M_u [(1 + \frac{1}{2}(\frac{l_p}{H_{tot}})^3 - \frac{3}{2}(\frac{l_p}{H_{tot}})] \quad (9)$$

$$l_p = 2H_{tot} \cos(\frac{\phi}{3} + \frac{4}{3}\pi), \cos\phi = \frac{1}{2}(\frac{M_y}{M_u} - 1) \quad (10)$$

lp: Length of the plastic hinge
l'p: Height of region over which reinforcement has yielded

2.2 Reinforced Concrete Structural Capacity Curve

The structural capacity curve is a plot based on the base shear V_b and the maximum roof displacement Δ , which is obtained from the superposition of the wall capacity curves. The bilinear wall capacity curve is defined by three parameters of the wall shear capacity V_m , the yield displacement over the wall Δ_y , and the final displacement over the wall Δ_u . In the following, the method of determining the capacity curve for structural wall systems with frame action due to the coupling of the walls is explained.

The range of the coupling effect is expressed by a parameter that is called zero moment height [1], which is a function of the spandrel flexural stiffness of the wall flexural stiffness $(EI_{sp} / l_0) / (EI_p / h_{st})$. Considering h_0 is the height of zero moment and M_u is the ultimate bending capacity of the wall, the shear capacity and yield displacement over the wall are determined by the following equations:

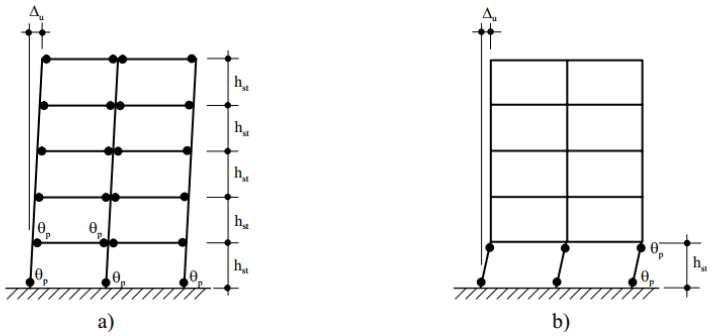

Figure 3: Ultimate displacement for (a) the spandrel mechanism, (b) the pier mechanism [1].

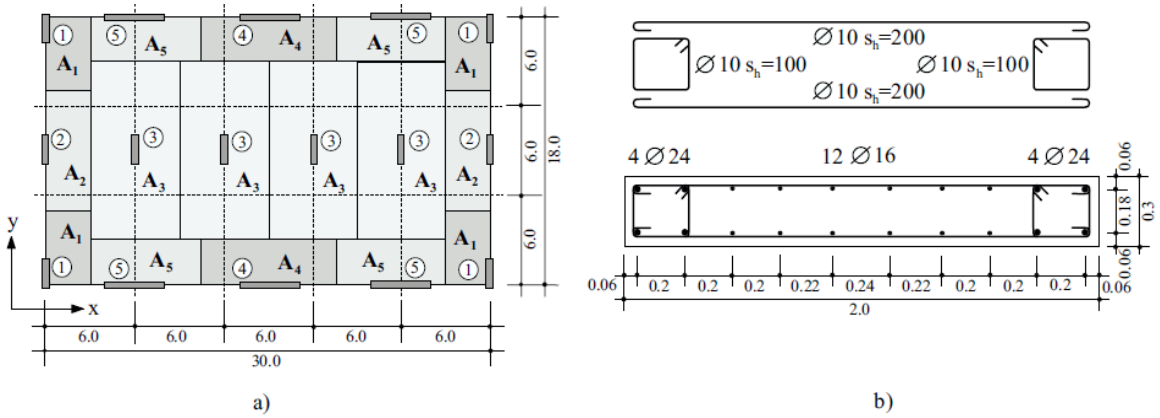

Figure 4: Building detail (a) building plan, and (b) structural walls details in y-direction [1].

$$V_m = \frac{M_u}{h_0} \quad (11)$$

$$\Delta_y = V_m H_{tot} \left(\frac{h_p(3h_0 - h_p)}{6EI_{eff}} + \frac{K}{GA_{eff}}\right) \quad (12)$$

The second part of the Eq. (12), shear ductility, is usually negligible. Given the Fig. (1), the effective stiffness of the cracked section can be determined based on the moment-curvature curve:

$$EI_{eff} = \frac{M_y}{\varphi'_y} \quad (13)$$

The ultimate displacement at top of the wall Δ_u is a function of the rotational ductility μ_φ and the type of mechanism. Depending on the bending strength, joints may be formed in the spandrel or the pier [3].

In the spandrel mechanism (Fig. 3 (a)) and the pier mechanism (Fig. 3(b)), the ultimate displacement is obtained from the following equations [1]:

$$\Delta_{u,ssm} = \Delta_y + (H_{tot} - \frac{l_p}{2})\theta_p = \Delta_y + (nh_{st} - \frac{l_p}{2})(Q_u - Q_y)l_p \quad (14)$$

$$\Delta_{u,psm} = \Delta_y + (h_{st} - \frac{l_p}{2})\theta_p = \Delta_y + (h_{st} - \frac{l_p}{2})(Q_u - Q_y)l_p \quad (15)$$

With the insertion of the Eq. (12), for Δ_y and ignoring the shear ductility, the ductility of the structural wall, for a combination of spandrel mechanism and the pier mechanism is equal to [3]:

$$\mu_w = 1 + (\mu_\varphi - 1)\frac{6h_0 l_p}{H_{tot} h_p (3h_0 - h_p)}(\beta h_{st} - \frac{l_p}{2}), 1 \le \beta \le n \quad (16)$$

In this way, the parameters defined in the bilinear capacity curve is determined by the coupling action. Building capacity curve is obtained in one direction from the superposition of the capacity curves of the walls in that direction.

Table 1: Material property used in the building.

Structural Element	$E_S\,(GPa)$	$f_y\,(MPa)$	$E_C\,(GPa)$	$f'_c(MPa)$
Wall	210	500	37.5	45
floor	210	460	30	28

Table 2: Summary of results for 3 structural walls in y-direction [1].

Wall	h_0 / h_p	$M_Y\,(kN.m)$	$\varphi_Y\,(1/m)$	$M_U\,(kN.m)$	$\varphi_U\,(1/m)$	μ_φ	l_p	$EI_{eff}\,(MN.m^2)$	$V_m\,(kN)$
1	1.7	5955	0.0025	7318	0.0179	7.29	0.54	2980	1266
2	1.7	3521	0.0026	5279	0.0306	11.83	1.029	2043	863
3	1.8	3034	0.0026	4786	0.0285	10.87	1.12	1824	782

Wall	$\Delta_y\,(mm)$	$\Delta_{u,psm}\,(mm)$	$\Delta_{u,ssm}\,(mm)$	$k_{eff}\,(KN.m)$
1	68	94	236	18494
2	73	155	640	11015
3	74	157	650	10545

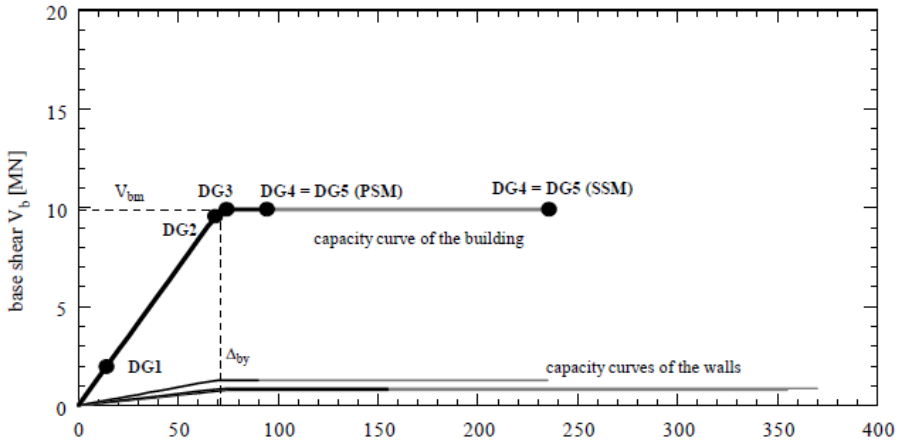

Figure 5: Capacity curve of reinforced concrete structure in y-direction [1].

Table 3: Summary of results for three types of structural walls in y-direction [1]

Wall	3	2	1
$V_{cr}(kN)$	465	199	148
$\Delta_{cr}(mm)$	25	17	14

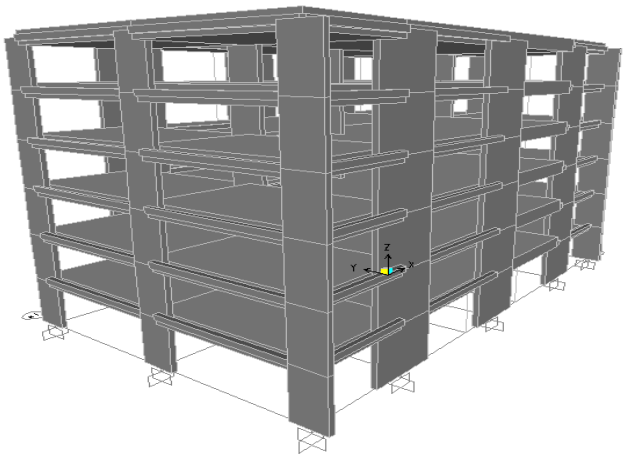

Figure 6: 3D view of the numerical model.

3. CASE STUDY BUILDING

Fig. 4 shows a 6-story concrete building with structural walls. Each floor has a height of 3.4 meters and sixteen walls. Material properties are presented in Table 1. These walls are classified into five types (A1 to A5), according to their positions and loading levels. The thickness of the slabs is 24 cm and the depth of the beams under the floor is 40 cm in the wall axis. The load on the floor is assumed to be 12.5 kN/m^2 by considering the wall weight. All existing walls in y-direction have a length of 2 meters, which is shown in its structural detail Fig. 4 (b). In Table 1, and Table 2, material properties and a summary of the results based on the presented equations for three types of walls in the y-direction are presented. Therefore, the bilinear capacity curves of these walls can be extracted, and consequently, the bilinear capacity curve of the building is obtained in the y-direction with superposition (Fig. 5) [1].

3.1 Damage Definition in Accordance with European Macroseismic Scale (EMS)

Five levels of vulnerability are defined for the reinforced concrete structures, which are determined as specific points on the bilinear capacity curve of the structure [1].

Damage level 1: At this stage, minor structural and nonstructural damages are observed. In fact, at this stage, cracks appear at the base of the walls. To determine this stage, the shear force, in which the first cracks appear, is calculated from the capacity curve. The critical moment (Mcr) occurs in Wall No. 1 is 905 kN, at the depth of 1.2 m ($x_{cr} = 1.2m$). The following results are obtained for the walls in the y-direction, using the presented equations (Table 3). Therefore, in the smallest displacement, which is in Wall No. 1, the first crack $(\Delta_{cr} = 14mm)$ appears. Thus, the sum of V_{cr} is obtained for all the walls $(V_{cr} = 1960kn)$. Moreover, the coordinate of Dcr=14mm and Vcr=1960 kN on the capacity curve represents the point at which the building enters in the first stage of damage (Fig. 5).

Damage level 2 is a moderate damage which is defined as a level that partial structural damage and moderate non-structural damage occur. In fact, at this stage, the damage appears as the cracks in the structural walls. Before this stage, the behavior of the structure is linear and at this stage, the building starts to behave nonlinearly. To determine the coordinate of the capacity curve, the displacement where the first wall enters into the yielding stage $(\Delta_{y,\min})$ is used, which is related to Wall No. 3 $(\Delta_{y3} = 68mm)$. The base shear for this displacement is 9570 kN (Vb=9570 kN). Therefore, the mentioned point with a displacement of 68 mm and a load of 9570 kN is the location on the curve where the structure has entered into the damage level 2 (Fig. 5).

Damage level 3 is the severe damage initiation which moderate structural damage and severe non-structural damage happen. At this stage, a spalling of concrete and buckling of reinforcements occurs. The structure extends into the nonlinear region and finally the last wall yields. This degree of damage is determined by the capacity curve from the largest displacement of walls yield ($\Delta_{y,\max}$) which is related to Wall No. 1 ($\Delta_{y1} = 74mm$), and the corresponding base shear is 9918 kN. At this point, the structure is in the damage level 3 (Fig. 5). According to Table 2, the stiffness of the building in the y-direction is 139785 kN/m. The amount of displacement at the point of yield is obtained, given the total shear force $V_b = 9918kn$, with the assumption of the linearity of the capacity curve before the yield.

$$\Delta_{by} = \frac{V_{bm}}{K} = \frac{9918}{139785} \times 10^3 = 71mm$$

Damage level 4 is the severe damage which includes severe structural and non-structural damages. In this stage, the first structural wall reaches its ultimate displacement. This stage is determined by the smallest ultimate displacement of the wall, which is corresponding to Wall No. 3 ($\Delta_{u3} = 94mm$). The pier mechanism with the coordinates of $(94mm, 9593kn)$ and spandrel mechanism with the coordinates of $(236mm, 9593kn)$ indicate the points on the capacity curve, which the structure enters the fourth degree of damage.

Damage level 5 is structural collapse which includes very severe structural damages. At this stage, the building is collapsed. It happens when the last wall reaches its ultimate displacement. At this time, the base shear of the building will be reduced to less than two-thirds of its maximum. Therefore, points $(94mm, 9593kN)$ and $(236mm, 9593kN)$ indicate coordinates of damage levels 4 and 5, respectively (Fig. 5).

3.2 Numerical modeling

SAP2000 program was used to conduct the nonlinear static analysis for the building [22]. The column elements are used to model the structural walls [23]. Thus P-M interaction diagrams are produced for each column element. The floor diaphragms of the building are assumed to be rigid. Due to the problems related to numerical convergence, the columns and wall elements were divided into three parts. The shear and flexural hinges are considered in the numerical model as well. For the elements of the column and wall, the flexural hinges are assigned at the relative distance of 0.05 of the length of the elements at each end. The shear hinges are assigned in the middle of the element length. The beams and the coupling

beams are modeled as frame elements with bending and shear hinges.

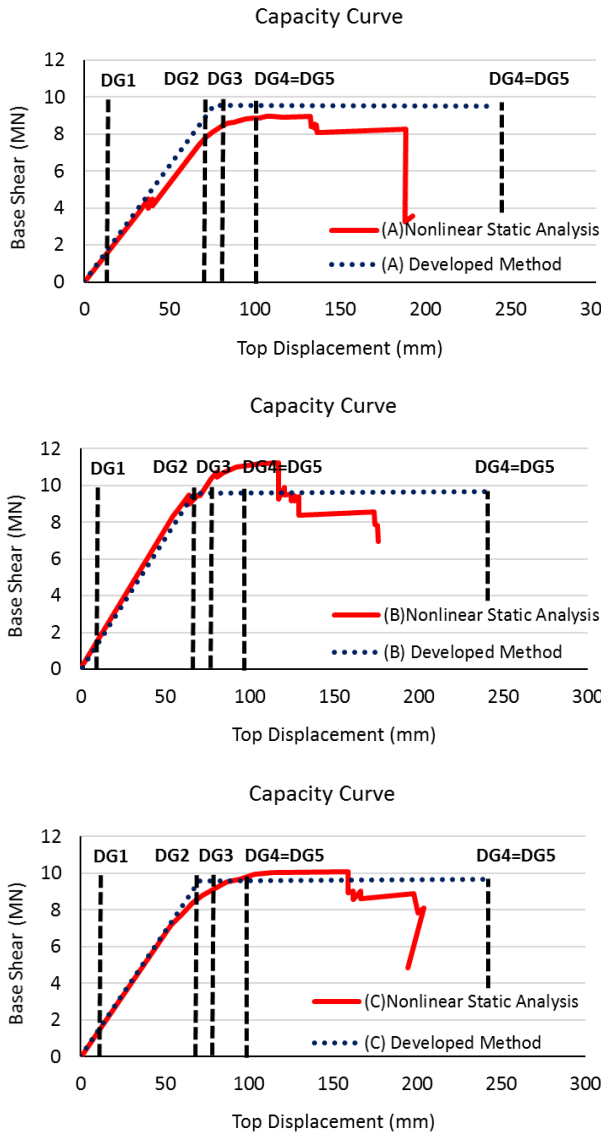

Figure 7: Capacity curves under different load patterns: (A) uniform acceleration, (B) IBC, and (C) first mode.

The numerical model subjected to three different lateral load patterns including uniform acceleration, IBC lateral load distribution, and first mode of vibration. After performing nonlinear static analysis, the structural capacity curves were extracted as shown in Fig. 7. The resulted capacity curves show a good agreement between the results of nonlinear static analysis under different lateral load patterns and the developed method by Swiss Federal Institute of Technology.

4. CONCLUSION

1. The capacity curve resulted from the uniform acceleration load pattern shows more vulnerability than the developed method by Swiss Federal Institute of Technology.

2. The capacity curve resulted from the IBC lateral load distribution shows less vulnerability than the developed method by Swiss Federal Institute of Technology.

3. Comparing between capacity curves obtained from the developed method by the Swiss Federal Institute of Technology and the nonlinear static analysis for all considered lateral load patterns shows that the proposed method appropriately estimates the capacity curve of concrete reinforced building with coupling between pier and spandrel.

4. Using structural walls with the frame action due to coupling behavior between the spandrels and piers can be considered as a reliable earthquake resisting system for high seismic regions for carrying the lateral and gravity load.

5. REFERENCES

[1] Swiss Federal Institute of Technology, 2002, Seismic vulnerability of existing building, Zurich.

[2] Oskouei, V.A. and Mahdavifar, V., 2013. Modeling of Two-Cell Concrete Cores for Investigation of Reliability of Equivalent Column Method.

[3] Mahdavifar, V., 2017. Cyclic performance of connections used in hybrid cross-laminated timber (Ph.D. dissertation), Oregon State University, Oregon, USA.

[4] Mahdavifar, V., Barbosa, A., Sinha, A., Muszynski, L. and Gupta, R., 2017. Hysteretic behaviour of metal connectors for hybrid (high-and low-grade mixed species) cross laminated timber, WCTE 2016 World Conference on Timber Engineering, Vienna, Austria.

[5] Belejo, A. and Bento, R., 2016. Improved modal pushover analysis in seismic assessment of asymmetric plan buildings under the influence of one and two horizontal components of ground motions. Soil Dynamics and Earthquake Engineering, 87, pp.1-15.

[6] Soltangharaei, V., Razi, M. and Gerami, M., 2016. Comparative Evaluation of Behavior Factor of SMRF Structures for Near and Far Fault Ground Motions. Periodica Polytechnica. Civil Engineering, 60(1), p.75.

[7] Soleimani, S., Aziminejad, A. and Moghadam, A.S., 2018. Approximate two-component incremental dynamic analysis using a bidirectional energy-based pushover procedure. Engineering Structures, 157, pp.86-95.

[8] Fanaie, N. and Ezzatshoar, S., 2014. Studying the seismic behavior of gate braced frames by incremental dynamic analysis (IDA). Journal of Constructional Steel Research, 99, pp.111-120.

[9] Soltangharaei, V., Razi, M. and Gerami, M., 2015. Behaviour factor of buckling restrained braced structures for near and far fault ground motions. International Journal of Structural Engineering, 6(2), pp.158-171.

[10] Chomchuen, P. and Boonyapinyo, V., 2017. Incremental dynamic analysis with multi-modes for seismic performance evaluation of RC bridges. Engineering Structures, 132, pp.29-43.

[11] Mahdi, T. and Gharaie, V.S., 2011. Plan irregular RC frames: comparison of pushover with nonlinear dynamic analysis. Asian J Civil Eng Build Housing, 12(6), pp.679-690.

[12] Yahmi, D., Branci, T., Bouchaïr, A. and Fournely, E., 2017. Evaluation of behaviour factors of steel moment-resisting frames using standard pushover method. Procedia Engineering, 199, pp.397-403.

[13] Pan, X., Zheng, Z. and Wang, Z., 2017. Estimation of floor response spectra using modified modal pushover analysis. Soil Dynamics and Earthquake Engineering, 92, pp.472-487.

[14] Soltangharaei, V., Zarean, M., Mahdavifar, V., Taghinezhad, R. and Taghinezhad, A., 2017. Response Modification Factor for Cold-Formed Steel Structures Using Pushover Analysis. International Journal of Engineering Science, pp. 15875-15880.

[15] Li, S., Zuo, Z., Zhai, C. and Xie, L., 2017. Comparison of static pushover and dynamic analyses using RC building shaking table experiment. Engineering Structures, 136, pp.430-440.

[16] Taghinezhad, R., Taghinezhad, A., Mahdavifar, V. and Soltangharaei, V., Numerical Investigation of Deflection Amplification Factor in Moment Resisting Frames Using Nonlinear Pushover Analysis. International Journal of Innovations in Engineering and Science, pp. 1-7.

[17] Bocciarelli, M. and Barbieri, G., 2017. A numerical procedure for the pushover analysis of masonry towers. Soil Dynamics and Earthquake Engineering, 93, pp.162-171.

[18] Taghinezhadbilondy, Ramin. "Extending Use of Simple for Dead Load and Continuous for Live Load (SDCL) Steel Bridge System to Seismic Areas." (2016), Ph.D. dissertation.

[19] Azizinamini, Atorod, Aaron Yakel, Ardalan Sherafati, Ramin Taghinezhad, and Jawad H. Gull. "Flexible Pile Head in Jointless Bridges: Design Provisions for H-Piles in Cohesive Soils." Journal of Bridge Engineering 21, no. 3 (2016).

[20] Pham, Huy, Ramin Taghinezhad, and Atorod Azizinamini. Experimental Investigation of Redundancy of Twin Steel Box-Girder Bridges Under Concentrated Load. No. 17-03649. 2017.

[21] Mohammadi, Alireza, Jawad H. Gull, Ramin Taghinezhad, and Atorod Azizinamini. "Assessment and Evaluation of Timber Piles Used in Nebraska for Retrofit and Rating." (2014).

[22] Computers and Structures Inc. (CSI), SAP2000 Three Dimensional Static and Dynamic Finite Element Analysis and Design of Structures V8.4.5, Berkeley, California.

[23] Naeim, Farzad, ed. The Seismic Design Handbook. Springer Science & Business Media, 2012.

International Journal of Science and Engineering Applications
Volume 7–Issue 02, 08-19, 2018, ISSN:-2319–7560

Qualitative Contours: A New Geochemical Method for Preliminary Mineral Exploration

Mohammadreza Agharezaei
Department of Mining and Metallurgy Engineering, Amirkabir University of Technology (Tehran Polytechnic), Tehran, Iran

Hossein Hajari
Department of Mining Engineering, University of Birjand, South Khorasan Province, Birjand, Iran

Ardeshir Hezarkhani
Department of Mining and Metallurgy Engineering, Amirkabir University of Technology (Tehran Polytechnic), Tehran, Iran

Abstract: The target in this paper is introduction and application of a new exploration method to locate and highlight mineral deposits and mineralization trends. Generally exploration methods could be categorized into two major groups; quantitative and qualitative methods. Although many attempts have been taken to progress the first group, the second one has not been considered and improved as it should have been. This research offers a new method named 'Qualitative Contours' which is descriptive rather than being numeric. This new method is applied to delineate mineralization trends and deposits locations in Qaleh-Zari area. The selected study area is located north west of Qaleh-Zari copper deposit. This area is selected to determine how effective this method is to find mineralization trends and the known Qaleh-Zari deposit. Theis new method "Qualitative Contours" successfully located Qaleh-Zari deposit and mineralization trends in the area. Beside the main function of this method, other beneficial performances are discussed such as lithology modeling and erosion levels estimation which are highly correlated to field observations in the area. In this research, locating the well-known Qaleh-Zari copper deposit as the result of the Qualitative Contours method is discussed and in order to prove the accuracy of such locating, Concentration-Volume (C-V) Fractal modeling is used to prove copper anomalies numerically.

Keywords: Qualitative contours, descriptive data, Exploration method, geochemistry, (C-V) Fractal, Qaleh-Zari

1. INTRODUCTION

Mining activities especially copper mining in Iran are based on thousands of years ago. According to Khoei et al.[1] several copper ore bodies are recognized in Iran (more than 500 or so). Different zones of copper ore bodies are suggested by researchers. Bazin and Hubner [2] suggested five zones. Khoei et al.[1] suggested six copper ore bodies in Iran as illustrated in Figure 1.

Delineation of geochemical anomalies from background is one of the major targets in exploration geochemistry. In order to achieve this goal, different descriptive and quantitive methods have been employed [3]. All of these methods are quantitative including statistical procedures, Fractal/multi-fractal modeling, neural network methods and other common methods which are being used as well by the researchers and experts.

In this study, a new method named "qualitative contours" is introduced. This method is proposed and employed to recognize mineralization trends and deposits locations in the study area. Qualitative contours would be a pioneer for introduction and application of descriptive data in exploration activities generating valuable results with low costs. The simplicity in method application and result interpretation are the other features persuading experts to use this method. The application and results of this new method on Qaleh-Zari copper deposit are discussed in this paper. Fractal/multi-fractal modeling is used in this study in order to check and compare the results. Fractal modeling was firstly introduced by Mandelbort [4] and then developed by Cheng et al. [5] and Li et al. [6].

2. GEOLOGY

2.1 Regional geology

The geology of Iran is represented by an assembly of continental fragments initially rifted from Gondwana land. As the Paleotethys and Neotethys oceans developed and closed, the fragments subsequently amalgamated [7-12]. The geological studies and tectonic researches of Iran date back to more than five decades [13-25]. It can be claimed that Iran owns one of the most variable and complex conditions in the world from the view point of economic geology. Approximately most of the known metallic and nonmetallic mining resources observed in Iran are economic.

Urmieh-Dokhtar magmatic belt in Tertiary caused several ore deposits in Iran especially copper deposits such as Porphyry and Skarn deposits [27-37]. The other recognized copper deposit types in Iran are volcanic massive sulfide (VMS) and Hydrothermal vein type deposits. The Lut block and its contact with the other blocks around it could be mentioned as

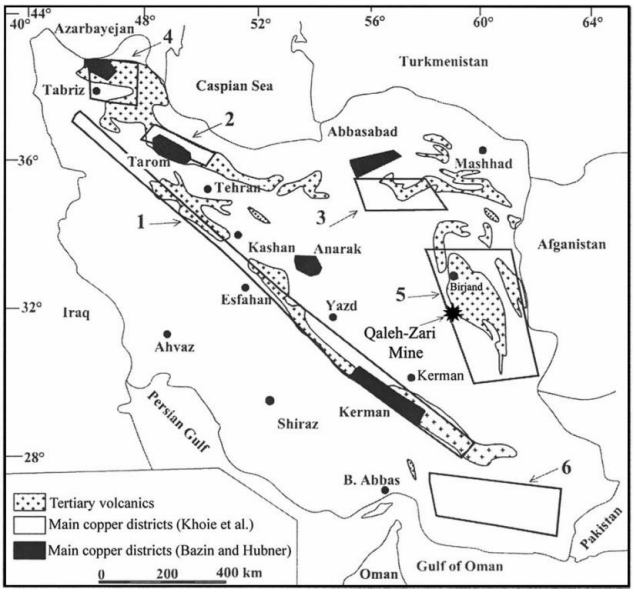

Fig. 1. The main zones of copper mineralization in Iran: (1) Orumieh-Dokhtar Belt; (2) Western Alborz Zone; (3) Kavir-Sabzevar Zone; (4) Sabalan; (5) Lut area; (6) Makran area [26]

one of the major locations for the VMS and hydrothermal vein type copper deposits. Figure 2 clearly demonstrates several Copper (Cu) and Lead-Zinc (Pb-Zn) mineralization localities in the Lut block.

2.2 Qaleh-Zari copper deposit

Qaleh-Zari copper deposit in the center of the Lut block is one of the most important copper deposits in Iran. Although the tonnage is low, the copper grade is high enough to assume Qaleh-Zari ore body as the noticeable one in Iran. This copper deposit is located 180km southwest of Birjand city [26] as demonstrated in figure 1. Qaleh-Zari deposit, like most of the copper deposits in Iran, has been mined since more than 2000 years ago. Historic mining around the deposit is significant. It is worth mentioning that these historic mining activities were the most important exploration clues in the area. Qaleh-Zari is a Fe-oxide Cu-Ag-Au vein type deposit [38].

Generally in hydrothermal vein type deposits structure of the area is the controller of hydrothermal fluids movement direction. The relationship between hydrothermal ore deposits and discontinuities in the crust (faults, fractures and lineaments) evokes that this deposit type is spatially consistent to regional structural features [40-63]. NW-SE and E-W trending could be considered for faults and fractures in this deposit, which also are the general structural trending in the whole area.

Qaleh-Zari copper deposit is located in the Lut block.

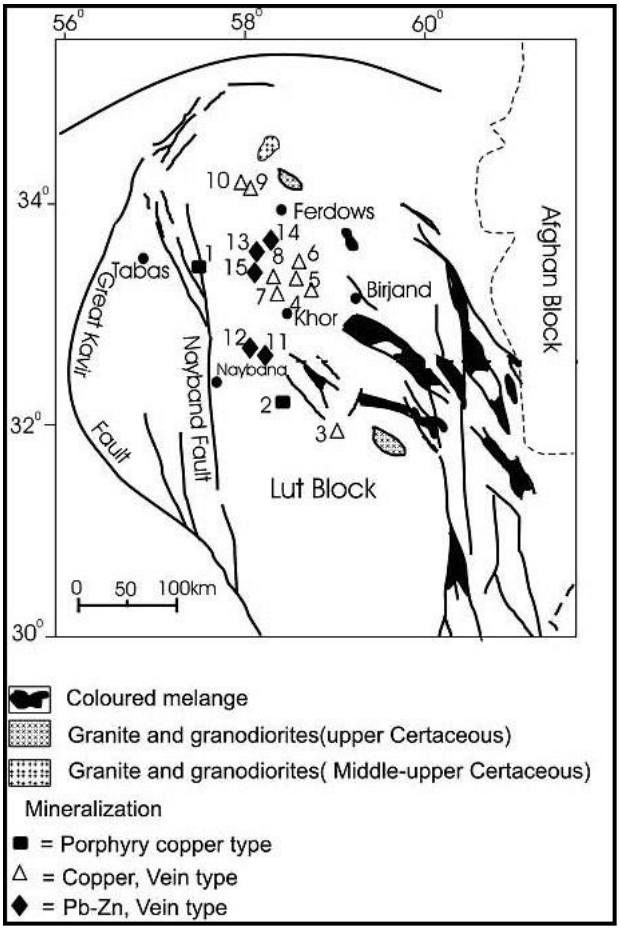

Fig. 2. Map of Cu, Pb-Zn mineralization localities in the Lut block. 1-Gazu, 2-Sorkh-Kuh, 3-Qaleh-Zari, 4-Howze Dough, 5-Ghare Kaftar, 6-Shurk, 7-Shikasteh Sabz, 8- Mire Khash, 9-Madan-e-Rahi I, 10-Madan-e-Rahi II, 11- Sehchangi, 12-Howze Rasi, 13-Shurab, 14-Gale Chah, and 15- Chah Nogre [39]

According to Daymehvar [64], the oldest formations are sedimentary rocks in the area. Paleogene volcanic rocks consist of high potassium calc-alkaline andesites (subduction zone shoshonites), andesitic basalts, dacites and rhyolites, andesitic and dacitic tuffs and pyroxene-bearing andesites [65- 67]. Basaltic rocks are the most abundant rock units in the area. Andesine and Andesitic basalt are the other major rock types observed in Qaleh-Zari area (Fig.3).

2.3 MINERALIZATION

A plutonic mass as the engine of a water circulation system has just created primary hydrothermal mineralization. Meteoric water plays an important role in enrichment and alteration processes in deposits associated with faults and fractures. Surface water flows can penetrate to deeper parts through the fractures. This process causes copper oxide minerals. The main copper mineral in Qaleh-Zari deposit is chalcopyrite.

According to the deposit type, a variety of paragenesis minerals are expected and also observed. Beside

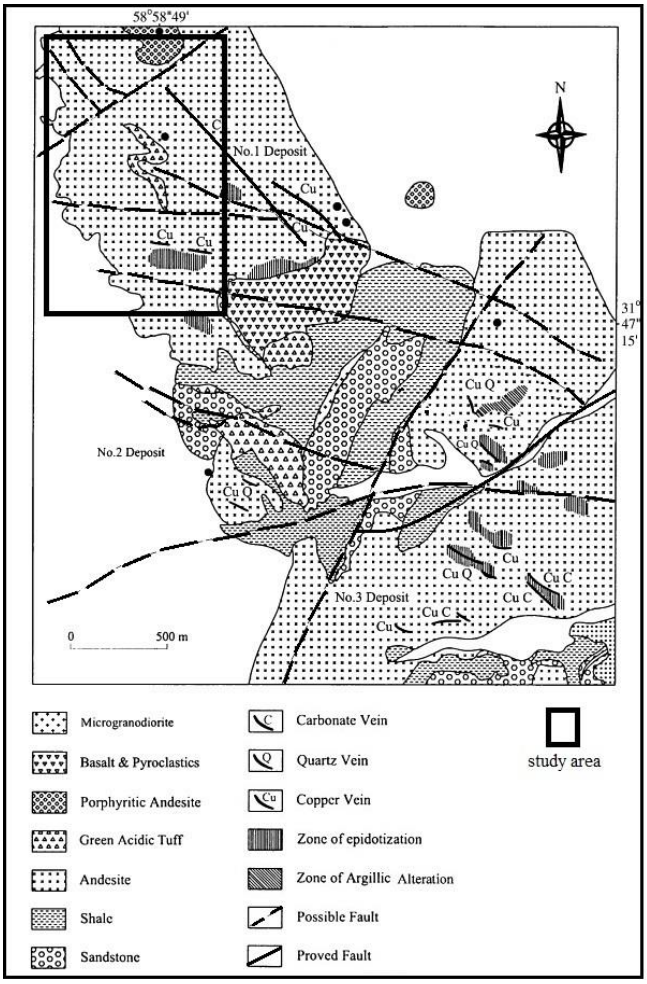

Fig.3 Geological Map of Qaleh-Zari Copper deposit (modified after Suzuki et al. [66] by Hassan-Nezhad and Moore [26])

chalcopyrite as the economic mineral, bornite, pyrite, hematite, galena, sphalerite, in sulfide supergene zone and malachite and aurite, in oxide supergene zone are the most common minerals in association with Quartz veins.

Four types of alterations are seen in Qaleh-Zari deposit. According to Hassan-Nezhad and Moore [26], these four alterations types are introduced as 1. sericitization; 2. argillization; 3. propylitization; and 4. Silicification.

2.4 Structural geology

In Qaleh-Zari deposit, mineralization is controlled by structural settings including faults and fractures with specific trending (NW-SE and E-W trending). İn hydrothermal deposits, structure of the deposit is very important to be studied since the mineralization is controled by the amount of fractures voulume which permits the hydrothermal fluid to pass through. The Qaleh-Zari deposit is a fissure-filling polymetallic vein system formed by hydrothermal solutions circulating through fault planes and breccia zones [65], [67] and [68]. In this deposit, major and minor fractures within which copper mineralization has occured are created as the result of a Right-sided compressive shear deformation system with N135 general trending [69]. Faults and fractures can be grouped into the following orientations:

1. NW– SE, these right-lateral high angle faults (dipping about 868) host the main ore-bearing veins. Dilation in these faults sometimes reaches up to 70 cm. 2. NE – SW, these barren fractures are younger than the other faults and fractures and show left-lateral movement. Locally, these fractures are seen to cut and displace ore-bearing veins, which occur along the oldest faults. 3. N – S, these fractures are the least common. Mineralization along these fractures is very poor and there is no evidence of mining along them. At the surface they are mostly mineralized by quartz and hematite. 4. E – W, faults from the point of view of mineralization are similar to Group 1 faults [26].

Based on the geological map (Fig.3) the study area includes NW-SE faults. It is noticeable that this trend for faults and fractures is controlling the mineralization in the area. Along the faults in the study area, copper mineralization is observed. These fractures are supposed as the most important structural features for mineralization in the study area. Thus sampling for the following method is mostly concentrated around these fractures.

3. METHODOLOGY

3.1 Qualitative Contours method

This method is devised and proposed by the authors of this paper for the first time. The primary targets of this new method are locating deposits and highlighting mineralization trends in study areas. The basis of this method is field observations. In other words, minerals, alterations and host rock observations are the input data which are recognized and recorded on the field. Exploration methods could be categorized in two major groups, quantitative and qualitative methods. Although many attempts have been taken to progress the first group, the second one has not been considered and improved as it should have been.

Generally field observations consists a bulk of geological datasets which could be categorized in several types such as structural features, mineralogy, surface and underground water conditions, chronology and etc.

This method is supposed to delineate mineral deposits and mineralization trending in the area of study. Among the possible field observations mentioned above, mineralogy of the study area is the research subject of this method. Firstly before using this method, the area must be selected for a special element (target element). In the other words, the target element defined in primary exploration studies is what the researchers look for economical minerals of (oxide, sulfide and other forms). The other factor is paragenesis minerals. Paragenesis minerals for the target element (or mineral) are very important. Most of the time, paragenesis minerals are the best guidance leading to locate the specific mineralization or ore deposits. Alterations, as an important characteristic, play a critical role in exploration process. Most mineral deposit types and the all of hydrothermal deposits include alterations extended inside or around the deposit. The alterations and their specific minerals would be the third answer key for locating deposits. The last but not least is the host rock. The host/barren rocks, extending in the area and surrounding mineralization, are principle objects to be distinguished. The host rock types could be easily recognized in geological maps since the most extended and abundant rock types with obvious trending usually are the host rock of mineralization in the area.

These four factors (1- economic target minerals, 2- paragenesis minerals, 3- alterations and 4- host rock) are the required field observations and the input data in Qualitative Contours method.

The data, as discussed above, is obtained from sampling on the field. Since there is no need to chemical analysis and the data is qualitative, just noting the observed minerals, alterations and host rock samples with the sampling location, is enough to create data set. It is recommended to observe at least 30 points in the area (thirty points are recomended as minimum number of samples needed to be considered as a statistical population as in classic statistics and also to make it possible to study the samples by classic statistics). The more samples the more accuracy in final results. There is no need to systematic sampling and also no force to scan and sample the whole area.

The next step is turning qualitative data into quantitative form. To achieve such goal, Table.1 is suggested. According to this table, the value for each sampling point could be defined. For illustration, the sampling point with economic target minerals is valued 4 scores and another sample point including any type of alterations in accordance to the target mineralization, is valued 2 scores. The same procedure for all the observation points is applied. Then these points and their values are plotted on a map based on the coordination of each sampling point. Thus the map includes some points (sampling points) with values 1, 2, 3 or 4. By supposing these values as Z value (Height) for each point, then it is possible to use these points to emerge a contour map (the first contour map). This contour map includes major contour lines (contour values 1, 2, 3 and 4).

Table1. Values for each type of observations (no dimension)

Observation types	Value
Host rock (1st type)	1
Alterations (2nd type)	2
Paragenesis minerals (3rd type)	3
Economic target minerals (4th type)	4

Based on the samples, several poles or peak points may appear on this contour map. The poles or peak point's value is 4. The poles are surrounded by other major contours. Each pole has an effective distance which separates it from other poles on the map. In this method enclosed area with contours 3 and 4 should be calculated. Then this calculated area is divided to the area of the whole region which is being studied. In the other words, the ratio of the enclosed area with contours 3 and 4 to the area of the whole study region should be calculated. This ratio value will be related to the poles of the map. This operation is critical because it creates dimensionless numbers and the dataset will be normalized to the total possible value (Total area) of the dataset. Then the value for each pole is a percent of the total area enclosed with contours 3 and 4 around the pole. In the next step, the value of each pole (the ratio value) will be related to the poles. A new contour map (Mineralization trend map) could be created for these poles based on their values. The mineralization's trending will be obviously recognizable in this map which could be demonstrated as arrows drawn from the center of areas enclosed with low contour values to the center of areas enclosed with high contour values.

The other noticeable feature of the first contour map is modeling the rock types of the whole area. There is no need to clarify that there are infinite numbers between two single numbers. Thus between 1, 2, 3 and 4 (the

observation type values) there are several definable numbers. As an example it is possible to define 2.5 between 2 and 3 then the contour value of 2.5 (between the two major contours 2 and 3) suggests mineralogy phase between alterations and paragenesis minerals. This is extendable to other minor contours determined by any interval number for the contour map.

These are not the only performances of these contours. The other beneficial one is using the map to estimate erosion levels in the area. Erosion levels are important factors for deposit position evaluation. The contours exactly suggest what should exist on the field then if there would be any differences with the contour map suggestions and field observations, erosion levels must be determined. In the other words, the differences mean that the expected mineralogy/lithology type has been eroded or burred previously. This method in this feature is highly more effective than a lithological map. Although in order to create a lithological map the whole areas and the whole rock unites and outcrops must be considered, there is no need to sampling the whole area for creating a qualitative contour map suggested by this study.

The contours (in the first contour map) created in this way evoke that the points are fractally distributed. To prove this claim, concentration-area (C-A) Fractal modeling has been applied for the areas enclosed by the qualitative contours. Since both methods are envolved with contours and surfacial study, fractal modeling is used. Concentration-area (C-A) Fractal modeling is introduced and expressed by Cheng et al. (1994) as: A (p) denotes the area with concentration values greater than the contour value p. This implies that A (p) is a decreasing function of p. If v represents the threshold, the following empirical model generally provides a good fit to the data for different elements in the study area:

$$A(p \leq v) \propto p^{-\alpha_1}; \quad A(p > v) \propto p^{-\alpha_2}$$

Where $\propto$ denotes proportionality.

3.2 Concentration-Volume (C-V) Fractal modeling

Concentration-volume (C-V) fractal modeling is similar to concentration-area (C-A) fractal modeling with the difference that instead of enclosed area, the volume is employed so the final result is expected to be a 3D anomaly model. This method is expressed as the following statements:

$V(\rho \leq v) \propto \rho^{-a1}$; $V(\rho \geq v) \propto \rho^{-a2}$

where $V(\rho \leq \upsilon)$ and $V(\rho \geq \upsilon)$ represent the two volumes with concentration values less than or equal to and greater than or equal to the contour value ρ; υ represents the threshold value of a geological zone (or volume);and a1 and a2 are the characteristic exponents. The break points in Log-Log plot in this method could be assumed as threshold values for geochemical populations. Based on the break points, background and anomaly are distinguished.

4. DISCUSSION

4.1 Qualitative contours method application

In this research, the new introduced method (Qualitative Contours method) is applied on Qaleh-Zari area (including Qaleh-Zari deposit) and the results are discussed. As mentioned before, Qualitative Contours method is kind of empirical procedures meaning that field observation (mineralogical/lithological features) are the input data.

In Qaleh-Zari area, the prospecting element or the target element is Copper. In the other words, locating copper mineralization is the goal of the study in this area and this research. To achieve this goal, the authors represent and suggest the new method Qualitative Contours. To begin with, 80 surface samples are collected from an area of about $46km^2$ north of Qaleh-Zari deposit. Mineralogical/lithological observations and location coordinates for each sample are recorded. According to the basis of Qualitative Contours method, the samples are categorized in four types. Some of the samples containing copper minerals (malachite, azurite, copprite) are grouped as the 4th type. Other samples in which paragenesis minerals for copper mineralization (magnetite, specularite, pyrite and gallena) are found are the 3rd type. As the same procedure, samples with any type of alterations (propylitic, silicic, argillic and potassic) excluding copper minerals or copper paragenesis minerals are the 2nd group and host/barren rock samples form the 1st type. The samples credited based on table 1 are plotted according to their coordinates and then the contour map is created in Surfer.11 software (Fig.4).

At the first look, each contour line recommends an equal feature for the points on it like any other contour map. This qualitative contour map suggests constant mineralogy/lithology for each contour line. In order to control the accuracy of the map, authors followed all major contours on the field according to the map (Fig.4). The result was extremely correlated to what the map was predicting. The qualitative contours not only do define different mineralogy/lithology types in the

area but also demonstrates geological features especially faults and fractures along the contours lines. Since this method is based on mineralogy and minerals are usually deposited along the fractures and faults,

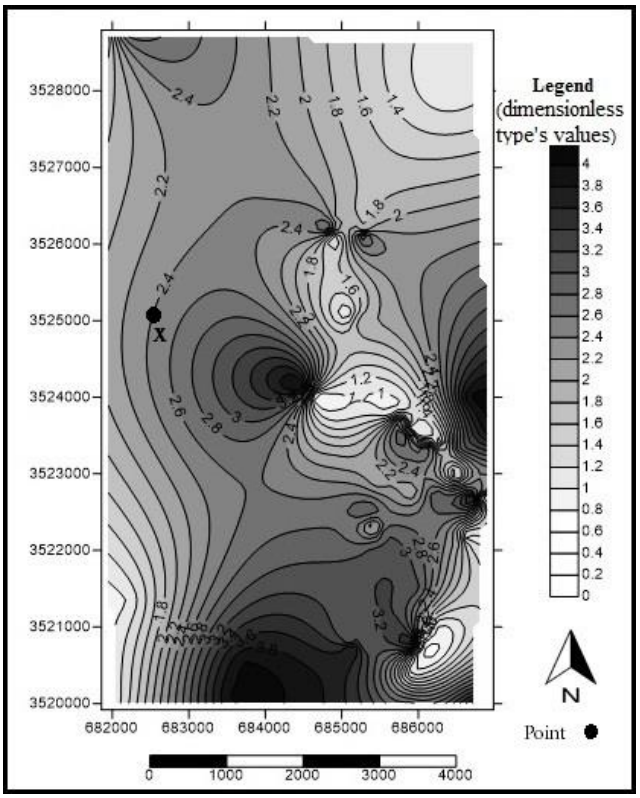

Figure 4. Contour map based on Qualitative contours method, X is an accuracy check point observed after runing the method.

when minerals observation locations are taken into account, the faults and fractures will be automatically mapped in mineralization maps along the mineralization trends and in addition, based on field observations in the area, the faults and fractures where oriented along the contours in figure4. Figures 5a and 5b show areas delineated by qualitative contours method as 4th and 1st types respectively.

As illustrated in figure 5a, copper-included quartz veins could be obviously distinguished on the surface. This vein is exactly located as contour value 4 in the qualitative contours map. Figure 5b shows basaltic host rocks in the area and it worth mentioning that their contour value on the qualitative contours map is 1 which proves the accuracy of the map.

The other aspect to point out is erosion level. Based on the qualitative contours map, erosion levels and conditions could be relatively determined. According to the qualitative contours map (Fig.4), in the point X, the contour value is 2.4 but instead of semi altered basalt (equivalent to contour 2.4 in the area), sediment in water stream is observed. This stream has created a valley between two hills that the qualitative contours map shows a constant value (similar mineralogy/lithology) for both hills. It means that previously there was the same mineralogy/lithology, as the two hills, in the point X before the stream activity

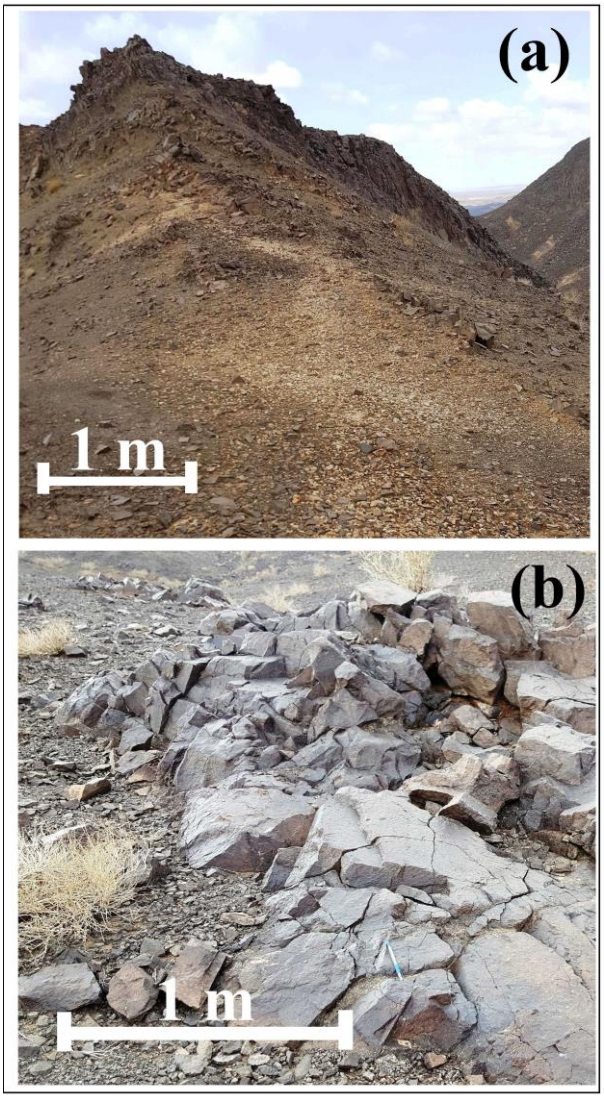

Figure 5. Field observations based on qualitative contours map. a) silicified veins including malachite, b) host rock outcrops

causing erosion in this point. This story is extensible to parts of the area with differences in qualitative contours value and field observations.

As another approach to this method, enclosed area by contour lines is the subject. In this method type 3 and type 4 (based on table 1) are claimed as anomalous segments of the dataset. The definition of anomaly in this case is the mineralization occurrence. In the other words, it is expected that this method demonstrates and highlights mineralized areas. One of the most frequently used methods to delineate anomalies related to enclosed areas by contour lines is Concentration-Area (C-A)

Fractal modeling. This method is applied to the areas enclosed by qualitative contours. The Log-Log plot (Log (value)-Log (area)) (Fig.6) shows a major breakpoint in 0.48 which is equal to 3.019 if antilog function be applied. It means points with values greater than 3.019 are the anomalous samples so based on table 1, 1st and 2nd types are background and 3rd and 4th types are anomalous data. Thus this method is highly correlated to the well-known Concentration-Area (C-A) Fractal modeling since both methods are suggesting the same anomaly threshold.

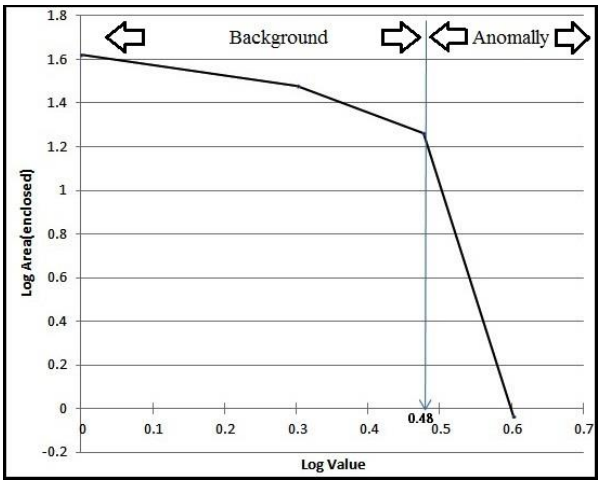

Figure 6. Log (value)-Log (area) plot based on (C-A) Fractal modeling

In addition, Mineralization trend map creation is possible by the use of qualitative contours map. As described in methodology section, enclosed area for contours 3 and 4 in the map (Fig.4) is calculated for each pole and is divided to the area of the whole study region. The result is a dimensionless value related to each pole. Then the contour map (Fig.7) is created in Surfer.11 software. This contour map is the Mineralization trend map. This map shows mineralization trend in the area increasing from north to south since the ratio percentage (enclosed area of contours 3 and 4 to the area of the whole region) increases.

This mineralization trend map suggests a mineralization gradient in the area. Based on the map, Southern parts are more potential for copper mineralization. It worth mentioning that Qaleh-Zari copper deposit is exactly located in southern regions out of the map. As a result, mineralization trend according to the Qualitative Contours method is just directing to the most mineralized area which would be very useful in the primary exploration steps.

4.2 Anomaly accuracy check

In this study, Qaleh-Zari area is investigated. The Qualitative Contours method is used and applied to an area located north of the deposit to see whether this method is capable to recognize the deposit. Since the method successfully worked, Qaleh-Zari deposit is the

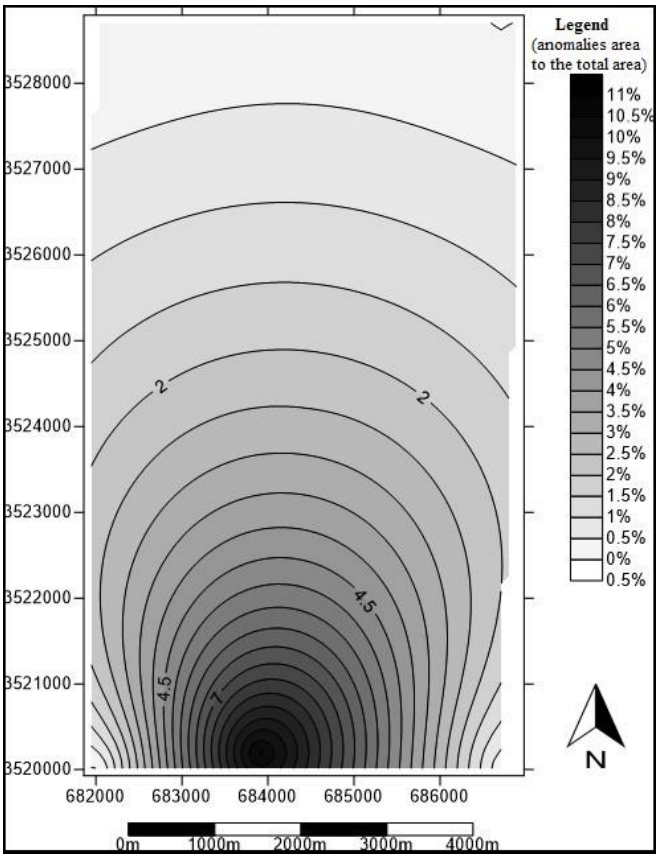

Figure 7. Mineralization trend map based on the Qualitative Contours Method.

next case study to prove the accuracy of geochemical copper anomalies suggested by the Qualitative Contours method in southern parts of the mineralization trend map (Fig.7) which is well-known Qaleh-Zari deposit. To determine copper geochemical anomaly in Qaleh-Zari copper deposit, 20 boreholes are drilled. The boreholes are drilled to simulate the condition that Qaleh-Zari deposit was not known for the researchers. This will control the results numerically. The cores obtained from the boreholes are used for sampling. In this case, 140 samples are derived from these boreholes and analyzed by ICP-MS (Inductively coupled plasma-mass spectrometry). The analysis result for copper is shown in table 2. To avoid large data table, only average copper content for each borehole is displayed in table 2.

Table 2. Boreholes average Cu content

Borehole number	Average Cu (ppm)
1	5-18
2	10-100
3	60-8100
4	1400-49500
5	20-400
6	40-5100
7	35-70
8	30-60
9	50-1000
10	2600-11000
11	30-89400
12	200-16900
13	30-90
14	40-12600
15	30-45
16	100-8300
17	22-3900
18	70-11000
19	1190
20	98-17500

Concentration-Volume (C-V) Fractal modeling is employed to define geochemical populations for the analysis results. To apply this Fractal method, volume per each grade is required. Thus the 3Dimentional model should be created. This model is created in Rockworks.14 software by Inverse Distance Weighting algorithm with cell size of 20 meters and then the volume per each grade is calculated. The Log-Log plot (Log (grade)-Log (volume)) (Fig.8) shows different geochemical populations in Qaleh-Zari copper deposit.

Based on the Concentration-Volume (C-V) Fractal modeling, anomaly threshold for copper samples is 1995ppm. This grade is applied to the 3Dimentional model of the deposit to create anomaly model (Fig.9).

According to the anomaly model, the economic copper deposit with threshold of 1995ppm is delineated and proved. Thus the Qualitative Contours method also is successful in locating mineral deposits as applied for Qaleh-Zari Copper deposit.

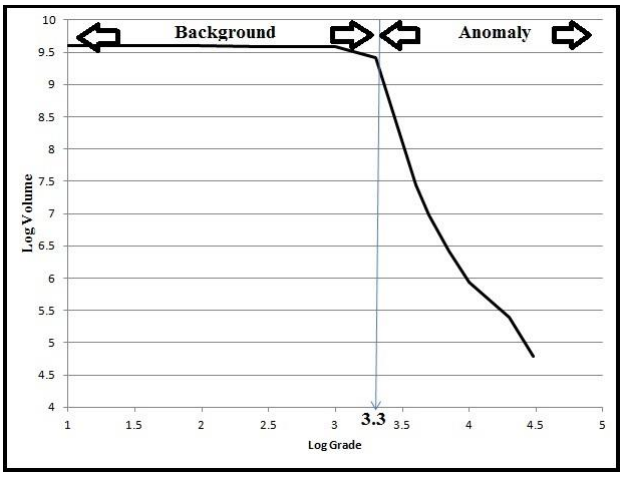

Figure 8. Log (grade)-Log (volume) plot based on (C-V) Fractal modeling.

5. CONCLUSION

Among different exploration methods, there are few procedures paying attention to qualitative data. Qualitative data arrangement is so much more cost and time effective than the so called quantitative datasets. Quantitative datasets include systematic sampling, expensive chemical analysis and complex data processing. The Qualitative Contours method introduced by this research opens the way forward to use qualitative and descriptive data. The data are based on field observations and there is no need to chemical analysis. This effective method is highly recommended in primary exploration steps and in projects with financial limitations. As discussed, this method is capable to delineate mineralization trends in a prospecting area which causes to locate mineral deposits.

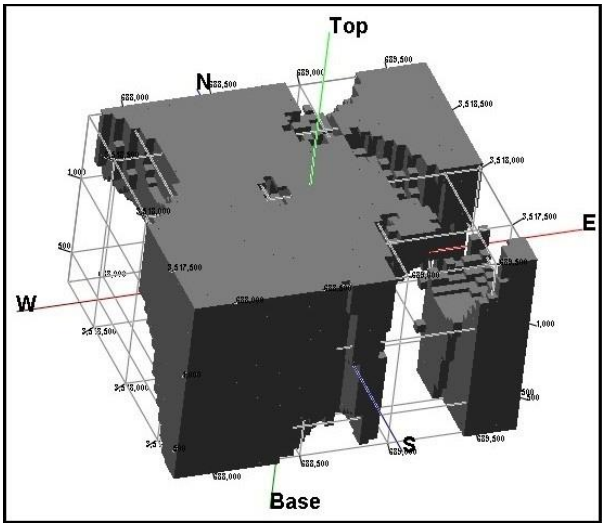

Figure 9. The 3Dimentional anomaly model of Qaleh-Zari deposit based on (C-V) Fractal modeling

The other important feature is the lithology modeling which the Qualitative Contours map suggests. According to the map, contours are defined as a type of mineralogy or lithology meaning that the type is constant on each single contour. This could be helpful and replaced to lithological map in a prospecting area since the contours are highly correlated to the geological field observations. Based on this fact, eroded unites in the area are easily recognized by the comparison between the qualitative contour map and the field observations. This method also is in high correlation to quantitative methods especially Fractal modeling. The anomalies based on both methods overlap each other that will encourage other researchers to use this new method for exploration purposes.

6. REFERENCES

[1] Khoei, N., Ghorbani, M., Taj-Baksh, P., 1999. Copper Deposits in Iran. GSI, Tarhe-Ketab (421 pp., (in Persian)).

[2] Bazin, D., Hubner, H., 1969. Copper deposits in Iran. Geological Survey of Iran, Internal Report No. 13, p. 195 (in English)

[3] Agharezaei, M. and Hezarkhani, A. (2016) Delineation of Geochemical Anomalies Based on Cu by the Boxplot as an Exploratory Data Analysis (EDA) Method and Concentration-Volume (C-V) Fractal Modeling in Mesgaran Mining Area, Eastern Iran. Open Journal of Geology, 6, 1269-1278.

[4] Mandelbort, B.B. (1982) The Fractal Geometry of Nature. Freeman, San Francisco, 460 p.

[5] Cheng, Q., Agterberg, F.P. and Ballantyne, S.B. (1994) The Separation of Geochemical Anomalies from Background by Fractal Methods. Journal of Geochemical Exploration, 51, 109-130. http://dx.doi.org/10.1016/0375-6742(94)90013-2

[6] Li, C., Ma, T. and Shi, J. (2003) Application of a Fractalmethod Relating Concentrations and Distances for Separation of Geochemical Anomalies from Background. Journal of Geochemical Exploration, 77, 167-175. http://dx.doi.org/10.1016/S0375-6742(02)00276-5

[7[Alavi, M., 1996. Tectonostratigraphic synthesis and structural style of the Alborz Mountains system in northern Iran. J. Geodyn. 11, 1–33.

[8] Berberian, M., King, G.C.P., 1981. Towards a paleogeography and tectonic evolution of Iran. Can. J. Earth Sci. 18 (2), 210–265.

[9] Meshkani, A., Mehrabi, B,. Yaghubpur, A., Sadeghi, M., 2013. 'Recognition of the regional lineaments of Iran: Using geospatial data and their implications for exploration of metallic ore deposits', *Ore Geology Reviews*, 55(0169-1368), pp. 48–63.

[10] Sengör, A.M.C., 1987. Tectonics of the Tethysides: orogenic collage development in a collisional setting. Annu. Rev. Earth Planet. Sci. 15, 213–244.

[11] Stocklin, J., 1968. Structural history and tectonics of Iran: a review. Am. Assoc. Petrol. Geol. Bull. 52, 1229–1258.

[12] Stocklin, J., 1977. Structural correlation of the Alpine ranges between Iran and central Asia. J. Geol. Soc. Fr. Mem. H. Ser. 8, 333 353.

[13] Stocklin, J., 1974. A-Northern Iran: Alborz mountains. Mesozoic – Cenozoic orogenic Belt, data for orogenic studies (Ed.), The TRANSMED Atlas: The Mediterranean Region from Crust to Mantle. Springer, New York, pp. 53–80. In: Spenncer, A.M. (Ed.), Geol. Soc., London, Sp. Pub4. Scottish Academic Press, pp. 213–234.

[14] Sengör, A.M.C., 1984. The Cimmeride orogenic system and the tectonics of Eurasia. Geol. Soc. Am. Spec. Pap. 195, 1–82

[15] Sengör, A.M.C., Altiner, D., Cin, A., Ustaomer, T., Hsu, K.J., 1988. Origin and assembly of the Tethyside orogenic collage at the expense of Gondwanaland. In: Audley- Charles, M.G., Hallaml, A. (Eds.), Gondwana and Tethys. Geol. Soc. Lond. Spec. Publ. 37, pp. 81–119.

[16] Davouzadeh, M., Schmidt, K., 1984. A review of the Mesozoic paleogeography and paleotectonic evolution of Iran. N. Jahrb. Geol. Palaontol. Abh. 68, 182–207.

[17] Kazmin, V.G., 1991. Collision and rifting in the Tethys Ocean: geodynamic implications. Tectonophysics 196, 371–384.

[18] Boulin, J., 1991. Structures in Southwest Asia and evolution of the eastern Tethys. Tectonophysics 196, 211–268.

[19] Alavi, M., 1994. Tectonic of the Zagros orogenic belt of Iran: new data and interpretations. Tectonophysics 229, 211–239.

[20] Ramezani, J., Tucker, R.D., 2003. The Saghand region, central Iran: U–Pb geochronology, petrogenesis and implications for Gondwana tectonics. Am. J. Sci. 303, 622–665.

[21] Stampfli, G.M., Borel, G.D., 2004. The TRANSMED transects inspace and time: constraints on the paleotectonic evolution of the Mediterranean domain. In: Cavazza, W., et al.

[22] Bagheri, S., Stampfli, G.M., 2008. A new litho-structural subdivision for the Palaeotethys terranes in central Iran (Anarak, Jandaq and Posht-e-Badamareas) and its geodynamic implications.

[23] Hassanzadeh, J., Stockli, D.F., Horton, B.K., Axen, G.J., Stockli, L.D., Grove, M., Schmitt, A.K., Walker, J.D., 2008. U–Pb zircon geochronology of late Neoproterozoic–Early Cambrian granitoids in Iran: implications for paleogeography, magmatism, and exhumation history of Iranian basement. Tectonophysics 451, 71–96.

[24] Omrani, J., Agard, P., Whitechurch, H., Benoit, M., Prouteau, G., Jolivet, L., 2008. Arcmagmatism and subduction history beneath the Zagros Mountains, Iran: a new report of adakites and geodynamic consequences. Lithos 106, 380–398.

[25] Agard, P., Yamato, P., Jolivet, L., Burov, E., 2009. Exhumation of oceanic blueschists and eclogites in subduction zones: timing and mechanisms. Earth Sci. Rev. 92, 53–79.

[26] Hassan-Nezhad, Ali A. and Farid Moore., 2005. "A Stable Isotope And Fluid Inclusion Study Of The Qaleh-Zaricu–Au–Ag Deposit, Khorasan Province, Iran". Journal of Asian Earth Sciences 27.6: 805-818.

[27] Forster, H., 1978. Mesozoic–Cenozoic metallogenesis in Iran. J. Geol. Soc. Lond. 35, 443–455.

[28] Hezarkhani, A., 2007. Geochemistry of the Enjerd skarn and its association with copper mineralization, northwestern Iran. Int. Geol. Rev. 48, 892–909.

[29] Hezarkhani, A., 2008. A fluid inclusion investigation hydrothermal evolution of the Miduk porphyry copper system, Kerman, Iran. Int. Geol. Rev. 50, 665–684.

[30] Karimzadeh Somarin, A., Moayyed, M., 2002. Granite- and gabbrodioriteassociated skarn deposits of NW Iran. Ore Geol. Rev. 20, 127–138.

[31] Mollai, H., Sharma, R., Pe-Piper, G., 2009. Copper mineralization around the Ahar batholith, north of Ahar (NW Iran): evidence for fluid evolution and the origin of the skarn ore deposit. Ore Geol. Rev. 35, 401–414.

[32] Shafiei, B., Haschke, M., Shahabpour, J., 2009. Recycling of orogenic arc crust triggers porphyry Cu mineralization in Kerman Cenozoic arc rocks, southeastern Iran. Miner. Deposita 44, 265–283.

[33] Shafiei, B., 2010. Lead isotope signatures of the igneous rocks and porphyry copper deposits from the Kerman Cenozoic magmatic arc (SE Iran), and their magmatic–metallogenetic implications. Ore Geol. Rev. 38, 27–36.

[34] Shahabpour, J., 1982. Aspects of alteration and mineralization at the Sar Cheshmeh copper–molybdenum deposit, Kerman, Iran. (Unpublished PhD thesis) Leeds University, Leeds, U.K.(342 pp.).

[35] Waterman, G.C., Hamilton, R.L., 1975. The Sar Cheshmeh porphyry copper deposit. Econ. Geol. 70, 568–576.

[36] Zarasvandi, A., Liaghat, S., Zentilli, M., 2005. Porphyry copper deposits of the Urumieh– Dokhtar magmatic arc, Iran. In: Porter, T.M. (Ed.), Super Porphyry Copper & Gold Deposits, A Global Perspective. PGC Publishing, Adelide (13 pp.).

[37] Zarasvandi, A., Liaghat, S., Zentilli, M., 2007. Geology of the Darreh-Zerreshk and Ali- Abad porphyry copper deposits, Central Iran. Int. Geol. Rev. 47, 620–646.

[38] Karimpour, M.A., Khin Zaw, D.L. Huston., 2005. 'S-C-O Isotopes, Fluid Inclusion Microthermometry, and the Genesis of Ore Bearing Fluids at Qaleh-Zari Fe-Oxide Cu-Au-Ag Mine, Iran', *Journal of Sciences, Islamic Republic of Iran*, 16(2)(1016-1104), pp. 153-168 (2005).

[39] Tarkian M., Lotfi M., and Baumann A. Magmatic copper and Lead Zinc ore deposits in the Central Lut, Eastern Iran. *N. Jb. Geol. Palaont. Abh*., **168**(2/3): 497-523 (1984).

[40] Bierlein, F.P., Murphy, F.C., Weinberg, R.F., Lees, T., 2006. Distribution of orogenic gold deposits in relation to fault zones and gravity gradients: targeting tools applied to the Eastern Goldfields, Yilgarn Craton, Western Australia. Miner. Deposita 41, 107–126.

[41] Grauch, V.J.S., Rodriguez, B.D., Bankley, V., 2003. Evidence for a Battle Mountain–Eureka crustal fault zone, north-central Nevada, and its relation to Neoproterozoic–Early Paleozoic continental breakup. J. Geophys. Res. 108 (B3), 2140.

[42] Groves, D.I., Vielreicher, R.M., Goldfarb, R.J., Condie, K.C., 2005. Controls on the heterogeneous distribution of mineral deposits through time. In: McDonald, I., Noyce, A.J., Butler, I.B., Herrington, R.J., Polya, D.A. (Eds.), Mineral Deposits and Earth Evolution: Geological Society, London, Special Publications, 248, pp. 71–101.

[43] Groves, D.I., Bierlein, F.P., 2007. Geodynamic settings of mineral deposit systems. J. Geol. Soc. 164, 19–30.

[44] Haynes, D.W., 2002. Giant iron oxide–copper–gold deposits: are they in distinctive geological settings? In: Cooke, D.R., Pongratz, J. (Eds.), Giant Ore Deposits: Characteristics, Genesis and Exploration. : CODES, Special Publication, 4. Hobart, Tasmania, pp.
57–77.

[45] Kerrich, R., Goldfarb, R.J., Richards, J., 2005. Metallogenic provinces in an evolving geodynamic framework. Economic Geology 100th Anniversary. 1097–1136.

[46] Sillitoe, R.H., 1972. Relation of metal provinces in western America to subduction of oceanic lithosphere. Bull. Geol. Soc. Am. 83, 813–818.

[47] Sillitoe, R.H., 2000. Gold-rich porphyry deposits: descriptive and genetic models and their role in exploration and discovery. Rev. Econ. Geol. 13, 315–345.

[48] Billingsley, P., Locke, A., 1941. Structure of ore districts in the continental framework. Am. Inst. Min. Metall. Eng. Trans. 144, 9 64.

[49] Kutina, J., 1969. Hydrothermal ore deposits in the western United States: a new concept of structural control of distribution. Science 165, 1113–1119.

[50] Kutina, J., 1971. The Hudson Bay Paleolineament and anomalous concentration of metals along it. Econ. Geol. 66, 314–325.

[51] Kutina, J., Fabbri, G., 1972. Relationship of structural lineaments and mineral occurrences in Abitibi area of the Canadian Shield. Geol. Surv. Can. Pap. 71-9, 36.

[52] Kutina, J., 1974a. Structural control of volcanic ore deposits in the context of global tectonics. Bull. Volcanol. 38, 1038–1069.

[53] Kutina, J., 1974b. Relationship between the distribution of big endogenic ore deposits and the basement fracture pattern. Examples from four continents. Proceedings of the First International Conference on the New Basement Tectonics: Utah Geol. Assoc. Publ., vol. 5, pp. 565–593.

[54] Kutina, J., 1975. Tectonic development and metallogeny of Madagascar with reference to the fracture pattern of the Indian Ocean. Bull. Geol. Soc. Am. 86, 582–592.

[55] Kutina, J., 1980. Regularities in the distribution of ore deposits along the Mendocino latitude Western United States. Global Tecton. Metallog. 1, 134–193.

[56] Kutina, J., 1983a. Global tectonics andmetallogeny; deep roots of some ore-concentrating fracture zones. A possible relation to small-scale convective cells at the base of lithosphere. Adv. Space Res. 3, 201–214.

[57] Kutina, J., 1983b. Similarities in the deep-seated controls of mineralization between the United States and China. Global Tecton. Metallog. 2, 111–142.

[58] Kutina, J., 1986. The role of basement tectonics in the distribution of some major ore deposits of Mesozoic and Cenozoic ages. In: Jiqing, Huang (Ed.), Proceedings of the Symposium on Mesozoic and Cenozoic Geology in Connection of the 60th Anniversary of the Geological Society of China.

[59] Kutina, J., 1988. Criteria indicating a block structure of the upper mantle and its role in metallogeny. Proceedings of the Seventh Quadrennial IAGOD Symposium, pp. 111–120.

[60] Favorskaya, M.A., Vinogradov, N.V., 1991. Geological evolution of ore-concentrating lineaments. Global Tecton. Metallog. 1 (1–2), 75–84.

[61] Richards, J.P., 2000. Lineaments revisited. Soc. Econ. Geol. Newsl. 42 (1), 14–20.

[62] Chernicoff, C.J., Richards, J.P., Zappettini, E.O., 2002. Crustal lineament control on magmatism and mineralization in northwestern Argentina: geological, geophysical, and remote sensing evidence. Ore Geol. Rev. 21, 127–155.

[63] Sillitoe, R.H., 2010. Porphyry copper systems. Econ. Geol. 105, 3–41.

[64] Daymehvar, M., 1996. Study of geology, mineralogy, geochemistry and genesis of Qaleh-Zari copper deposit. Unpublished MSc Thesis. Teacher Training University, p. 133 (in Farsi).

[65] Sadaghyani-Avval, F., 1976. Etude ge´ologique de la re´gion de la mine de Khal- Eh-Zari (Iran) mineralisation et inclusions fluids. Unpublished PhD Thesis, Universite´ de Nancy, Nancy, p. 165.

[66] Suzuki, Y., Ogawa, K., Akiyama, N., 1976. Copper ores from the Qaleh-Zari Mine, Iran. Mining Geology 385, 26–391.

[67] Moore, F., Hassan-Nezhad, A.A., 1994. Fluid inclusion study of mineralization at the Qaleh-Zari Mine, South

Khorasan, Iran. Iranian Journal of Science and Technology 18, 213–223.

[68] Karimpour, M.H., Zaw, K., 2000. Geothermometry and physicochemical condition of Qaleh-Zari Cu–Au ore bearing solution based on chlorite composition and fluid inclusion study. Iranian Journal of Crystallography and Mineralogy 8, 3–22 (in Farsi with English abstract).

[69] Khatib, M, M,. 1999. The relationship between shear deformation and mineral veins in Qaleh-Zari. In the congerence of recognition of mining potentials in eastern Iran, Birjand.

International Journal of Science and Engineering Applications
Volume 7–Issue 02, 20-22, 2018, ISSN:-2319–7560

An Eye Blink and Head Movement Detection for Computer Vision Syndrome

Vinaya Kulkarni
Department of Computer Engineering,
Bharati Vidyapeeth's College of Engineering for Women,
Dhankawadi, Pune, India

Chetana Thombre
Department of Computer Engineering,
Bharati Vidyapeeth's College of Engineering for Women,
Dhankawadi, Pune, India

Nehanaaz Shaikh
Department of Computer Engineering,
Bharati Vidyapeeth's College of Engineering for Women,
Dhankawadi, Pune, India

Tejashri Tarade
Department of Computer Engineering,
Bharati Vidyapeeth's College of Engineering for Women,
Dhankawadi, Pune, India

Tejaswini Patne
Department of Computer Engineering,
Bharati Vidyapeeth's College of Engineering for Women,
Dhankawadi, Pune, India

Abstract—The usage of computers in our day-to-day activities has increased enormously leading to both positive and negative effects in our lives. The negative effects are related to health problems such as Computer Vision Syndrome (CVS) etc. Prolonged use of computers would lead to a significant reduction of spontaneous eye blink rate due to the high visual demand of the screen and concentration on the work. The proposed system develops a prototype using blink as a solution to prevent CVS. The first part of the work captures video frames using web camera mounted on the computer or laptop. These frames are processed dynamically by cropping only the eyes, which determines the eye-status based on the threshold value and the proposed idea. Various experiments are done and their algorithms are compared and concluded that the proposed algorithm yields 99.95% accuracy.
Keywords: OpenCV, Computer Vision Syndrome, Haar Cascade.

1. INTRODUCTION

Computer Vision Syndrome

Computer became basic need for human. Almost all the task are completed using computer. These days, many of us have jobs that require us to stare at computer screens for hours at a time. That can put a real strain on your eyes. Medical study indicates an average adult blinks once in 4 seconds. When eye focuses on an object or pays more attention in activities such as reading, watching a video in a digitized environment the rate of blinking decreases to about 3 to 4 times per minute [2]. This transformation leads to a greater stress to the visual system leading to CVS .Also research shows that 40% to 80% have these symptoms. Eye problems caused by computer use fall under the heading computer vision syndrome (CVS). Prolong use of computer leads to, eye irritation, abnormal eye blink rate, head ache, blur eyes, neck and shoulder pain, itchy eyes, watery eyes.

The impact of the disease leads to poor visual functions, increased stress levels, reduced effective work hours, frequent absence from work, possible increase in errors, less time available for personal care and this in turn has reduced productivity. Thus confronting a solution has become the primary need. A lightweight product is expected with less execution time to adapt to the dynamic environment.

Amongst all these symptoms for computer vision syndrome, we are basically trying to focus on abnormal eye blink rate which will detect that the user has CVS and also focusing on the factor of abnormal head movement which shows that the user has neck pain, and also the third factor which is close eye duration which shows that the user is falling asleep due to strain in the eyes or constant use of computer. The proposed system will help to detect and prevent the symptoms of computer vision syndrome. The web camera captures the video and the frames are processed for detecting stress of eyes and head. OpenCv will first localize the head then will localize the eyes. OpenCv is also used for segmentation of head movement. Our system will calculate the eye blink rate, if it is greater or lesser than threshold value then Computer Vision Syndrome will be detected and for head movement detection if it is greater than threshold value then Computer Vision Syndrome will be detected. Then the system will generate the output as text to speech like stay alert or take a break.

2. LITERATURE SURVEY

2.1 Take-A-Break Notification by Nellmendee Julius, in 2014 is a software which runs on Windows operating system designed for office workers who have the highest tendency on prolonged computer screens use, in order to reduce Computer Vision Syndrome (CVS). The purpose of this study is to prevent computer users from looking in front of a computer screen for a long period of time. Rapid Application Development (RAD) methodology has been used for the project development phase.

2.2 Electrooculography Based Blink Detection Using Computer vision Syndrome by Monalisa Pall, Anwesha Banerjee in 2014 which proposes an artificial system capable of preventing Computer Vision Syndrome from the analysis of eye movements. Ocular data is recorded using an Electrooculogram signal acquisition system developed in the laboratory. Wavelet detail coefficients obtained using Haar

and Daubechies order 4 mother wavelets are used as signal features. From the recorded data, blinks are classified from any other type of eye movements using Support Vector Machine (SVM) classifier with different kernel functions. It obtain a maximum average accuracy of 95.83% over all classes and participants using second order polynomial kernel SVM classifier. Then the trained classifier has been used in real time to detect blinks. The system is designed to count the number of blinks in a particular interval of time thereby reminding people working on a computer for long periods to rest and blink frequently in case of insufficient number of blinks.

2.3 Close Faced-Distance Warning System for computer Vision Syndrome in 2015, Takeshi Toda, MasetoNakai, Xinxin Liu in which it proposes a close face-distance warning system in order to keep personal computer (PC) user away from to the PC display and to prevent straightened neck during prolong PC usage. The system estimates the distance between the display and the user face (called as face distance) from the user face area that is real-timely measured from captured image with built-in webcam. Haar-like cascade classifier is used for the facedetection and tracking from captured image every frame. The face distance is then estimated from the number of pixels of the detected skin color area. The system then shows a pop-upwarning message on the display when the face comes close to the display than a limit, in order to promote keeping face away from the display.

2.4 Web-based Content Management System Payal Wasnik, Amutha Jeyakumar have done a paper in 2016. In this, it remotely monitoring a patient's health condition is now easily possible with the use of sensors, actuators and mobile communication devices, combined together called as Internet of Things for Medical Devices. The ArduinoYun is a Microcontroller board having built-in Ethernet and Wi-Fi support and can be connected to a vast array of web-based Resource and services with the use of Temboo, a cloud-based platform with processes for APIs, databases, and more. The parameters considered under Ergonomic workspace like distance between user and computer, angle with which the computer screen should be positioned can be analysed using Ultrasonic And Accelerometer sensors; while pulse sensor to analyse heart rate under work pressure

3. PROPOSED SYSTEM

In this system , we have basically three modules,

3.1 Head Movement Detection :

Web Camera will capture the video and then it will convert these video into number of frames. Harcascade Algorithm is used for detection of head and eyes in this system. Using this frames OpenCV will localize the head and will localize the eyes. OpenCV is nothing but open source computer vision library, which is used for localization of moving object. This will give more clear images than colour models. It also used for segmentation of images. After localizing head, the system will calculate the head movement. We fixed the threshold value as >5 times in half an hour, that means if the end user will move his head more than 5 times in a such a way that it will cross the fixed range. This range is fixed by segmentation by using OpenCV. We consider left hand side and the right hand side range for segmentation. We will localize head and consider square area as per the user head size; this area will be range for detection of the head movement. If the head movement is not greater than threshold value, system will shift to next image. If the head movement is greater than threshold value then system will generate the output as take a break and be alert.

2.2 Eye Movement Detection :

The second part is detection of eyes. Using OpenCV we localize head and then will localize eyes. Until and unless the head is not localized the eye is not detected. In this modules there are two subparts where we consider the time of eye closed duration and blink rates . Normally the human eye blinks every 4 seconds. If the user will blink his eyes more or less than threshold value as 2-3 blinking per seconds then it will detect as computer vision syndrome. Because of low blinking rate user will face the eyes problems such as dry eyes, red eyes, and itchiness in eyes which are symptoms of computer vision syndrome. So if blinking rate is less or more than threshold value system will alert generate as take a break.

3.3 Eye Close Duration:

Sometimes, the blinking rate is very much low as user may get sleep while doing work on computer. So this will detect by the subpart as finding closed eye duration. If the end user will close his eyes more than 10 minutes, system will generate alert as be awake, stay alert. This will basically help the user to stay awake and do his/her work. So after getting alert from the system the end user will take break for some time or will more focus on work.

3. SYSTEM ARCHITECTURE

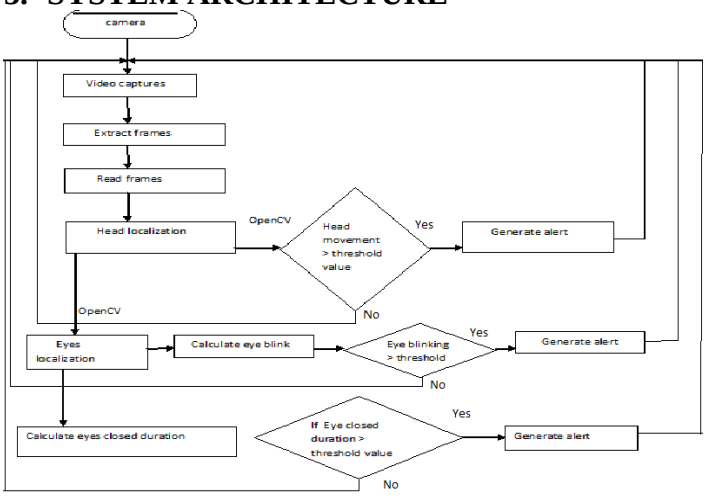

Fig 1.System Architecture

In System architecture, basically it shows :

4.1 Camera: It captures the video of an user who is sitting in front of the computer. Video gets captured and gets stored in the memory.

4.2 Frames Extraction: Once the video gets captured, the frames gets extracted from the video, and then are further processed.

4.3 Head Localization: Head is localized once the frame gets read , OpenCV localizes the head, if the head movement is abnormal , i.e. if it is more than the threshold value then the Computer Vision Syndrome is detected. It will then generate the alert, if it not detected then it will start to read the new frame.

4.3 Eye Localization: Head is localized once the frame gets read , OpenCV localizes the head and the eyes, if the eye movement is abnormal , ie if it is more than or less than the threshold value then the Computer Vision Syndrome is detected. It will then generate the alert, if it not detected then it will start to read the new frame again.

4.4 Closed Eye duration: Once the eye localization is done , if the users eye remains close more than the threshold value the , user gets an alert to stay awake or asked to take a break .

4.5 Generate Alert: Alert is generated if the computer Vision syndrome is detected.

Haar Cascade Algorithm

Object Detection using Haar feature-based cascade classifiers is an effective object detection method proposed by Paul Viola and Michael Jones in their paper, "Rapid Object Detection using a Boosted Cascade of Simple Features" in 2001. It is a machine learning based approach where a cascade function is trained from a lot of positive and negative images. It is then used to detect objects in other images.Here we will work with face detection. Initially, the algorithm needs a lot of positive images (images of faces) and negative images (images without faces) to train the classifier. Then we need to extract features from it. For this, haar features shown in below image are used. They are just like our convolutional kernel. Each feature is a single value obtained by subtracting sum of pixels under white rectangle from sum of pixels under black rectangle.

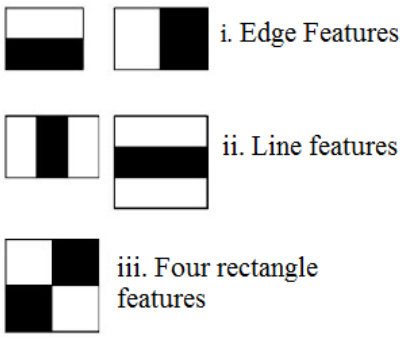

Fig 2. Haarcascade classifier

Now all possible sizes and locations of each kernel is used to calculate plenty of features. For each feature calculation, we need to find sum of pixels under white and black rectangles. To solve this, they introduced the integral images. It simplifies calculation of sum of pixels, how large may be the number of pixels, to an operation involving just four pixels. It makes things super-fast. But among all these features we calculated, most of them are irrelevant. For example, consider the image below. Top row shows two good features. The first feature selected seems to focus on the property that the region of the eyes is often darker than the region of the nose and cheeks. The second feature selected relies on the property that the eyes are darker than the bridge of the nose. But the same windows applying on cheeks or any other place is irrelevant. So how do we select the best features out of 160000+ features? It is achieved by Adaboost.

Haar-cascade Detection in OpenCV

OpenCV comes with a trainer as well as detector. If you want to train your own classifier for any object like car, planes etc. you can use OpenCV to create one. Here we will deal with detection. OpenCV already contains many pre-trained classifiers for face, eyes, smile etc. Those XML files are stored in opencv/data/haarcascades/ folder. Let's create face and eye detector with OpenCV.

Cascade Classifiers

The object recognition process (in our case, faces) is usually efficient if it is based on the features take-over which include additional information about the object class to be taken-over. In this tutorial we are going to use the Haar-like features and the Local Binary Patterns (LBP) in order to encode the contrasts highlighted by the human face and its spatial relations with the other objects present in the picture. Usually these features are extracted using a Cascade Classifier which has to be trained in order to recognize with precision different objects: the faces' classification is going to be much different from the car's classification.

4. ACKNOWLEDGMENTS

We would like to take this opportunity to express sincere thanks to the department and the University for this Course where we have such an opportunity to express our ideas and put our learning all the way into practice.

5. REFERENCES

[1] Sofia Jennifer J, Sree Sharmila T "Edge based Eye Blink detection For Computer Vision Syndrome" April 2017

[2] Takeshi Toda, Masako Nakai, Xinxin Liu, "A Close Face-Distance Warning System For Straightened Neck Prevention" November 2015

[3] Monalisa Pal, Anweesha Banerjee, "Electrooculography Based blink detection to computer Vision Syndrome" November 2014

[4] A. Banerjee, S. Chakraborty, P. Das, S. Datta, A. Konar, D.N .Tibarewala and R. Janarthanan, "Single channel electrooculogram(EOG) based interface for mobility aid" , Fourth International Conference on Intelligent Human Computer Interaction, 2012.

[5] Seongwon Han, Sungwon Yang, Jihyoung Kim and Mario Gerla , "EyeGuardian: A Framework of Eye Tracking and Blink Detection forMobile Device Users", HotMobile12 February 2829, 2012, San Diego,CA, USA.